Synopsis

Synopsis of thesis entitled **"Electrochemical Investigations Related to High Energy Li-O$_2$ and Li-ion Rechargeable Batteries"** by **Surender Kumar** (4110-112-101-08036) under the supervision of Prof. N. Munichandraiah, Department of Inorganic and Physical Chemistry, Indian Institute of Science, Bangalore (India), for the Ph.D. degree of the Institute under the Faculty of Science.

A galvanic cell converts chemical energy into electrical energy. Devices that carry out these conversions are called batteries. In batteries, generally the chemical components are contained within the device itself. If the reactants are supplied from an external source as they are consumed, the device is called a fuel cell. A fuel cell converts chemical energy into electrical energy as long as the chemicals are supplied from external reserves. The working principle of a metal-air battery involves the principles of both batteries and fuel cells. The anode of a metal-air cell is stored inside the cell, whereas O$_2$ for the air-electrode is supplied from either atmosphere or a tank.

There are several metal-air batteries available academically, which include Zn-air, Al-air, Fe-air, Mg-air, Ca-air, Li-air and Na-air batteries. So far, only Zn-air battery is successfully commercialized. Li-air battery is attractive compared to other metal-air batteries because of its high theoretical energy density (11140 Wh kg^{-1}). The energy density of Li-air battery is 3 - 5 times greater than state-of-art Li-ion battery. Li-air (or Li-O$_2$) battery comprises Li-metal as the anode and a porous cathode. The cathode and the anode are separated by a suitable separator soaked in an organic electrolyte. Atmospheric air can enter the battery through the porous cathode. Out of the mixture of gases present in the air, only O$_2$ is electrochemically active. For optimization purpose, most of researchers use pure O$_2$ gas instead of air. Li-air battery is not commercialized till now because of several issues associated with it. The issues include: (i) sluggish kinetics of O$_2$ electrode reaction, (ii) decomposition of the electrolyte during charge-discharge cycling, (iii) formation of Li dendrites, (iv) contamination by moisture, etc. Among these scientific and technical problems related to Li-O$_2$ cell system, studies on rechargeable O$_2$ electrode with fast kinetics of oxygen reduction reaction (ORR) during the cell discharge and oxygen evolution reaction (OER) during charge in non-aqueous electrolytes are important. In non-aqueous electrolytes, the 1-electron reduction of O$_2$ to form superoxide (O$_2^-$) is known to occur as the first step.

Subsequently, superoxide undergoes reduction to peroxide (O_2^{2-}) and then to oxide (O^{2-}). The kinetics of ORR is slow in non-aqueous electrolytes. Furthermore, the reaction needs to be reversible for rechargeable Li-air batteries. In order to realize fast kinetics, a suitable catalyst is essential. The catalyst should be bifunctional for both of ORR and OER in rechargeable battery applications. Noble metal particles have been rarely investigated as catalysts for O_2 electrode of Li-O_2 cells. Graphene has two-dimensional planar structure with sp^2 bonded carbon atoms. It has become an important electrode material owing to its high electronic conductivity and large surface area. It has been investigated for applications such as supercapacitors, Li-ion batteries, and fuel cells. Catalyst nanoparticles prepared and anchored to graphene sheets are expected to sustain discrete existence without undergoing agglomeration and therefore they possess a high catalytic stability for long term experiments as well as applications. In this context, it is intended to explore the catalytic activity of noble metal nanoparticles dispersed on reduced graphene oxide (RGO) for O_2 electrode of Li-O_2 cells. While a majority of the investigations reported in the thesis involves noble metal and alloy particles dispersed on RGO sheets, results on polypyrrole-RGO composite and also magnesium cobalt silicate for Li-O_2 system are included. A chapter on electrochemical impedance analysis of $LiMn_2O_4$, a cathode material of Li-ion batteries, is also presented in the thesis.

Introduction on electrochemical energy storage systems, in particular on Li-O_2 system is provided in the 1st Chapter of the thesis. Synthesis of Ag nanoparticles anchored to RGO and catalytic activity are presented in the 2nd Chapter. Ag-RGO is prepared by insitu reduction of Ag^+ ions and graphene oxide in aqueous phase by ethylene glycol as the reducing agent. The product is characterized by powder XRD, UV-VIS, IR, Raman, AFM, XPS, SEM and TEM studies. The SEM images show the layered morphology of graphene and TEM images confirm the presence of Ag nanoparticles of average diameter less than 5 nm anchored to RGO (Fig. 1a). Ag-RGO is investigated for ORR in alkaline (1 M KOH), neutral (1 M K_2SO_4) and non-aqueous 0.1 M tetrabutyl ammonium perchlorate in dimethyl sulphoxide (TBAP-DMSO) electrolytes. The ORR follows 4e⁻ reduction in aqueous and 1e⁻ reduction pathway in non-aqueous electrolytes. Li-O_2 cells are assembled with Ag-RGO as
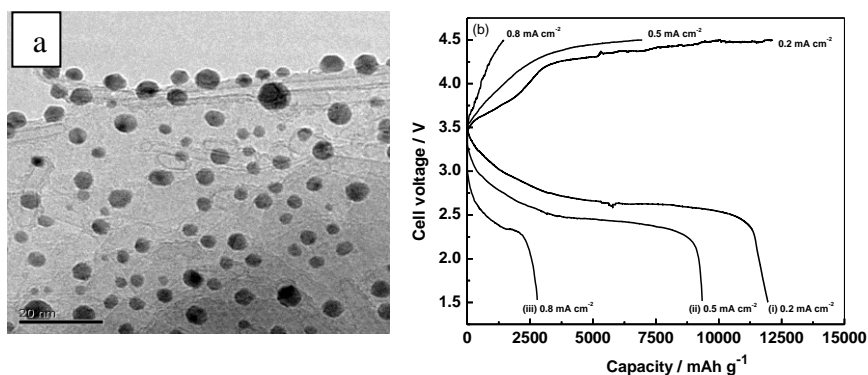
Fig. 1. (a) TEM image of Ag-RGO and (b) charge-discharge voltage profiles of Li-O$_2$ (Ag-RGO) cells.

oxygen electrode catalyst in non-aqueous electrolyte (1 M LiPF$_6$-DMSO) and subjected to charge-discharge cycling at several current densities. The discharge capacity values obtained are 11950 (11.29), 9340 (5.00), and 2780 mAh g^{-1} (2.47 mAh cm^{-2}) when discharged at 0.2, 0.5, 0.8 mA cm^{-2}, respectively (Fig. 1b). Powder XRD studies of discharged electrodes indicate the formation of Li$_2$O$_2$ and Li$_2$O during the cell discharge. In addition to these studies, Na-O$_2$ cells are also assembled with Ag-RGO in non-aqueous electrolyte. It is concluded that the chemistry Li-O$_2$ and Na-O$_2$ cells are similar except for the capacity values.

Metal nanoparticles of Au, Pd and Ir are decorated on RGO sheets by reduction of metal ions on graphene oxide by NaBH$_4$. Au-RGO, Pd-RGO and Ir-RGO are characterized by various physicochemical techniques. Particle size of metal nanoparticles ranges from 2 to
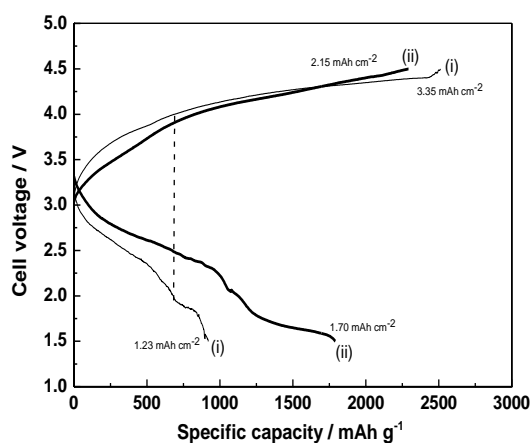

Fig.2. Charge-discharge voltage profiles Li-O$_2$(RGO) (i) and Li-O$_2$(Au-RGO) (ii) cells at current density 0.3 mA cm^{-2}.

(iii)

10 nm on graphene sheets. All samples are studied for ORR in aqueous and non-aqueous electrolytes by cyclic voltammetry and rotating disk electrode experiments. Li-O_2 cells are assembled in 1 M LiPF$_6$-DMSO and discharge capacity values obtained are 3344, 8192 and 11449 mAh g^{-1} with Au-RGO, Pd-RGO and Ir-RGO, respectively, at 0.2 mA cm^{-2} current density. The results of these studies are described in Chapter 3.

Synthesis and electrochemical activity of Pt-based alloy nanoparticles (Pt$_3$Ni, Pt$_3$Co and Pt$_3$Fe) on RGO are presented in Chapter 4. The Pt$_3$Ni alloy particles are prepared by simultaneous reduction of Pt^{4+}, Ni^{2+} and graphene oxide by hydrazine in ethylene glycol medium. Pt$_3$Co-RGO and Pt$_3$Fe-RGO are also prepared similar to Pt$_3$Ni-RGO. Formation of alloys is confirmed with XRD studies. O_2 reduction reaction on Pt-alloys in non-aqueous electrolyte follows 1e$^-$ reduction to O_2^-. RDE results show that Pt$_3$Ni-RGO is a better catalyst than Pt for O_2 reduction (Fig. 3). Li-O_2 cells are assembled with all samples and subjected to
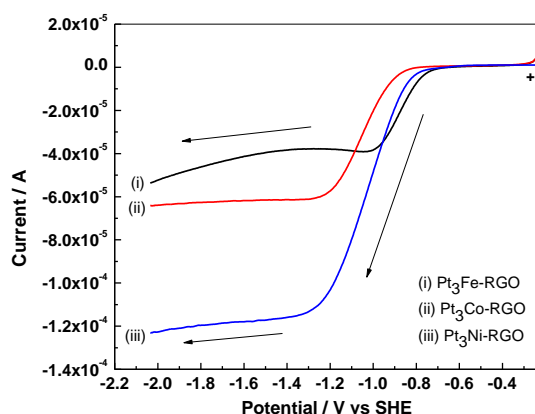

Fig. 3. *Linear sweep voltammograms of Pt$_3$Ni-RGO, Pt$_3$Co-RGO and Pt$_3$Fe-RGO in 0.1 M TBAP-DMSO with 1600 rpm at 10 mV s^{-1} scan rate. The area of GC electrode was 0.0314 cm^2 with a catalyst mass of 200 µg.*

charge-discharge cycling at several current densities. The initial discharge capacity values obtained are 14128, 5000 and 10500 mAh g^{-1} with Pt$_3$Ni-RGO, Pt$_3$Co-RGO and Pt$_3$Fe-RGO, respectively, as the air electrode catalysts.

Polypyrrole (PPY) is an attractive conducting polymer with advantages such as high electronic conductivity and electrochemical stability. A combination of advantages of graphene and PPY composite are explained in the Chapter 5. PPY is grown on already synthesized RGO sheets by oxidative polymerization of pyrrole in an acidic medium. RGO-

PPY composite is characterized by XRD and Raman spectroscopy studies. $Li-O_2$ cells are assembled in non-aqueous electrolyte and subjected for charge-discharge cycling at different current densities. The discharge capacity value of $Li-O_2$(PPY-RGO) cell is 3358 mAh g^{-1}
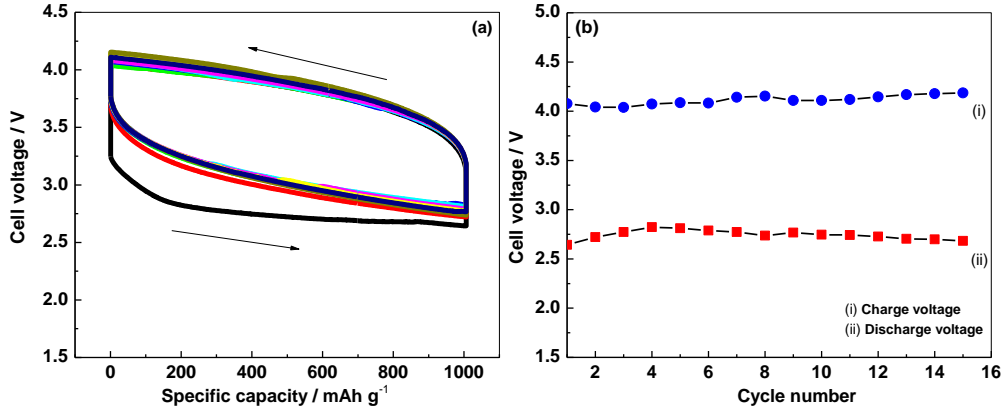

Fig. 4. *(a) Discharge-charge performance of Li-O$_2$(PPY-RGO) cell with a current density of 0.2 mA cm^{-2} limiting to a capacity of 1000 mAh g^{-1} and (b) variation of cut-off voltages on cycling.*

(3.94 mAh cm^{-2}) in the first cycle. $Li-O_2$(PPY-RGO) cell delivers 3.7 times greater discharge capacity than $Li-O_2$(RGO) cell. Cycling stability of $Li-O_2$ (PPY-RGO) cell is investigated by charge-discharge cycling by limiting the capacity to 1000 mAh g^{-1}, and the cell voltage at the end of discharge and at the end of charge are found constant at 2.75 and 4.10 V, respectively (Fig. 4 a, b). This study shows that PPY-RGO is stable in $Li-O_2$ cells. Electrochemical impedance study shows that charge-transfer resistant is 500 Ω for freshly assembled $Li-O_2$(PPY-RGO) cell and it decreases to 200 Ω after 1st discharge.

Synthesis of magnesium cobalt silicate and its electrochemical activity are presented in Chapter 6. $MgCoSiO_4$ is synthesized by mixed solvothermal approach and characterized by various physicochemical techniques. Cubic shaped $MgCoSiO_4$ is investigated for oxygen evolution reaction (OER) activity in alkaline and neutral media. The current values at 0.95 V versus SHE are 43, 0.18, 16 mA cm^{-2} on $MgCoSiO_4$, bare carbon paper and Pt foil electrodes, respectively (Fig. 5), indicating that $MgCoSiO_4$ is a good catalyst for OER. The onset potential for OER is 0.68 V versus SHE on $MgCoSiO_4$ in 1 M KOH. OER activity on $MgCoSiO_4$ is also studied in K_2SO_4 and phosphate buffer electrolytes. The results indicate good catalytic activity of $MgCoSiO_4$ in neutral electrolytes also. The catalytic activity of
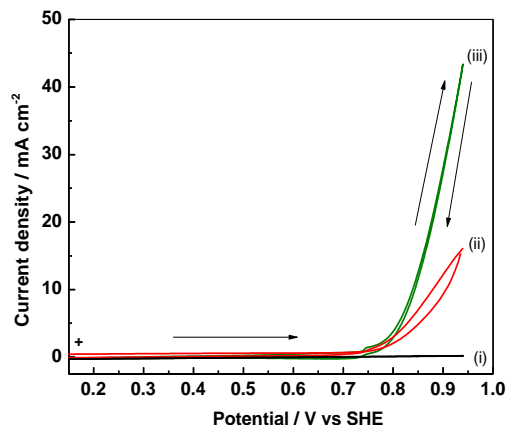
Fig. 5. *Cyclic voltammograms of bare carbon paper (i), Pt foil (ii), MgCoSiO$_4$ coated carbon (iii) electrodes in 1 M KOH (sweep rate = 5 mV s^{-1}, loading level = 1.15 mg, area = 0.5 cm^{-2}).*

MgCoSiO$_4$ towards ORR in aqueous and non-aqueous electrolytes is studied by RDE experiments. Li-O$_2$ cells are assembled with bifunctional MgCoSiO$_4$ catalyst in 1 M LiPF$_6$-DMSO electrolyte and the discharge capacity values obtained are 7721 (8.27), 2510 (1.66) and 1053 mAh g^{-1} (0.92 mAh cm^{-2}) when discharged at 0.3, 0.5 and 0.8 mA cm^{-2} current densities, respectively.

Electrochemical impedance spectroscopy (EIS) measurements of LiMn$_2$O$_4$ electrode are carried out at different temperatures from -10 to 50 ^{0}C and in the potential range from 3.50 to 4.30 V, and the data are analysed in Chapter 7. In the EIS spectra recorded over the frequency range from 100 kHz to 0.01 Hz at different temperatures, there are two semicircles present in the Nyquist plot (Fig. 6a). But in 3.90 to 4.10 V versus Li/Li$^+$(1M) potential range at low temperatures (-10 to 15 ^{o}C) range, another semicircle also appears (Fig. 6b). Impedance parameters such as solution resistant (R$_s$), charge-transfer resistance (R$_{ct}$), double-layer capacitance (C$_{dl}$), electronic resistance (R$_e$) and Warburg impedance (W$_R$), etc., are obtained by analysis of the EIS data. The variations of resistances with temperature are analysed by Arrhenius-like relationships and the apparent activation energies of the corresponding transport properties are evaluated. The values of activation energy for charge-transfer process are 0.37, 0.30 and 0.42 eV, at 3.50, 3.90 and 4.10 V versus Li/Li$^+$(1M), respectively. The chemical diffusion coefficient of Li$^+$ ions into LiMn$_2$O$_4$ calculated from EIS data. The values of diffusion coefficient calculated are in the range of 2.50 x 10^{-12} - 4.10 x 10^{-11} cm^2 s^{-1}.
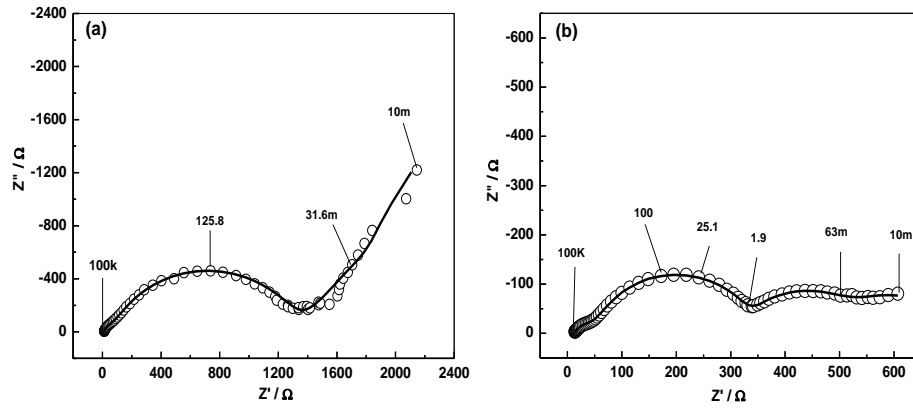
Fig. 6. *Nyquist plot of impedance study of Li/LiMn$_2$O$_4$ cell at 3.50 V (**a**) and 3.90 V (**b**) at -10 ^{0}C.*

Details of the above studies are described in the thesis.